Chapter 5

Microscopic Structure and Dynamics of Air/Water Interface by Computer Simulations and Comparison with Sum-Frequency Generation Experiments

The hydrogen (H) bonded structure of water at the air/water interface [155, 156, 157, 158, 159] is of fundamental interest because it determines the properties of aqueous interfaces and their reactivity. Certain atmospheric reactions [160], such as those involved in ozone depletion, are known to be catalyzed by the ice surface on cloud particles. Study of the air/water interface is also important for understanding more complicated organic/water interfaces [159] that have recently begun to attract interest for its potential for rate acceleration [161] of organic reactions and green chemistry in emulsions. For example, interest in catalytic effects of dangling OHs has also been extended to their role in catalysis of different organic reactions by metal oxides enriched in surface OH groups [162].

The first molecular structure of water at the air/water interface using the surfacespecific vibrational sum-frequency generation (SFG) technique was reported by Du et al. [163] in 1993 [155, 164] In that work, using the titration of dangling OH groups with methanol and hence the complete suppression of the peak of the free OH SFG signal, it was found that about 25% of surface water molecules have one dangling OH bond that is not H-bonded to other water molecules. It is thereby free, and protrudes out of the water phase, confirming earlier predictions from computations [165]. Roughly the same picture of the existence of the free OH bonds at the interface has since been consistently observed in SFG experiments by Richmond [159], Eisenthal [166], Allen [167], and Gan et al. [168], and also in computer simulations [157, 169, 170, 171, 172, 173] The structure of water at the hydrophobic organic/water interfaces was shown to be similar to that at the air/water interface [163, 174, 175]. In the process of understanding the air/water interface, different interpretations were also made in terms of details of the air/water interface using both experiments and computations [155, 176, 177, 178]. Although previous work has made significant progress toward explaining the observed SFG spectra using theory and simulation [159, 159, 179, 180, 181], a complete picture of how rapid motion averages out the SFG has not been presented. In the present chapter, we make a quantitative comparison between multiple experimental observables, going beyond the comparison of ratios. In addition, by utilizing independent experimental results, coupled with molecular dynamics simulation of the air/water interface, the present work has as a goal a better understanding of motional averaging in SFG. This study was prompted by the recent on-water catalysis experiments [161] and our interpretation in terms of the role of dangling OH groups at the wateroil emulsion interface [182].

The orientation of free OH bonds at the air/water interface has been deduced from several SFG experiments to be nearly perpendicular to the surface plane [163, 168, 183]. An SFG interpretation [183] assumed a step-like distribution for the tilt angles (θ_{OH}) between the free OH bonds and the surface normal, suggesting them to be in the interval $0° \leq \theta_{OH} \leq 51°$, yielding an average tilt angle $\theta_{OH} \approx 35°$. A more recent SFG experiment [168] yielded a similar average tilt angle, $\theta_{OH} \approx 30°$, with a narrow distribution width of $\leq 15°$, assuming a Gaussian distribution model. In contrast to these distributions and average orientations of free OH bonds, however, previous molecular dynamics simulations [157, 169, 159, 171, 172, 184] with various water models consistently predicted widths of the orientational distribution much broader than those assumed in the previous interpretations of SFG experiments [155, 163, 168, 183]. We address this discrepancy by considering the nature of free OH bonds on the surface, and, in a procedure detailed below, selectively removing those that would likely not contribute to the SFG, allowing a direct comparison between our calculations and experimental measurements.

5.1 Methods

The theoretical treatment we use in this chapter to calculate the effective SFG nonlinear susceptibilities originated from the one previously developed in the literature [163, 183] to extract the orientation information of interfacial molecules from SFG experiments. Previous reviews have provided details of the treatment [185, 186].

Here, we summarize the assumptions and key expressions, for completeness, and implement the expressions to obtain the forms that are suitable for numerical calculations of the mode amplitudes by explicit integrals, rather than the more simplified fast and slow approximations [183].

The SFG signal is proportional to the square of the effective nonlinear susceptibility, $\chi^{(2)}_{\text{eff}}(\omega)$, which is a sum of resonant, $\chi^{(2)}_{\text{R,eff}}(\omega)$, and nonresonant, $\chi^{(2)}_{\text{NR,eff}}(\omega)$, contributions [155]:

$$\chi^{(2)}_{\text{eff}}(\omega) = \chi^{(2)}_{NR,eff} + \chi^{(2)}_{R,eff} = \chi^{(2)}_{NR,eff} + \sum_{q} \frac{A_{q,\text{eff}}}{\omega - \omega_q + i\Gamma_q}, \tag{5.1}$$

where ω is the incident infrared, ω_q is the q^{th} vibrational frequency, $A_{q,\text{eff}}$ is the mode amplitude, and Γ_q is the damping constant for the q^{th} vibrational mode. The sum-frequency spectra are obtained by scanning the IR frequencies that probe the vibrational normal modes, using the IR-visible SFG method. The susceptibility originates at the air/water interface, caused by the symmetry breaking at the boundary. The bulk of the fluid has inversion symmetry and so does not contribute to techniques generating second-order nonlinear polarization.

SFG is approximated to be dipolar in origin, and we neglect any quadrupolar contribution that could emanate from the bulk [163]. In this paper we focus on the free OH stretching mode of water molecules at the air/water interface, $\omega_q = 3698$ cm^{-1}. This stretching frequency corresponds to the water configuration where one OH bond is free while the other OH bond of the same parent water molecule is still H-bonded to neighboring water molecules (so-called “single-donor” configuration). The spectra for the *ssp*, *ppp*, and *sps* combinations of polarization, labeled in the order of the sum frequency output, visible input, and infrared input fields, are obtained in SFG experiments.

The A_{eff}'s in eq. (5.1) can be related to the intrinsic tensor components via the Fresnel factors, i.e., via the macroscopic local field corrections, L_{ii} [185],

$$A_{\text{eff}}(ssp) = L_{yy}(\omega_s)L_{yy}(\omega_1)L_{zz}(\omega_2)\sin\beta_2 A_{yyz} \tag{5.2a}$$

$$\begin{aligned} A_{\text{eff}}(ppp) = &- L_{xx}(\omega_s)L_{xx}(\omega_1)L_{zz}(\omega_2)\cos\beta_s\cos\beta_1\sin\beta_2\, A_{yyz} \\ &- L_{xx}(\omega_s)L_{zz}(\omega_1)L_{xx}(\omega_2)\cos\beta_s\sin\beta_1\cos\beta_2\, A_{yzy} \\ &+ L_{zz}(\omega_s)L_{xx}(\omega_1)L_{xx}(\omega_2)\sin\beta_s\cos\beta_1\cos\beta_2\, A_{zyy} \\ &+ L_{zz}(\omega_s)L_{zz}(\omega_1)L_{zz}(\omega_2)\sin\beta_s\sin\beta_1\sin\beta_2\, A_{zzz} \end{aligned} \tag{5.2b}$$

$$A_{\text{eff}}(sps) = L_{yy}(\omega_s)L_{zz}(\omega_1)L_{yy}(\omega_2)\sin\beta_1\, A_{yzy}, \tag{5.2c}$$

where β_s, β_1, and β_2 are the reflected or incident angles of sum frequency output, visible input, and infrared input, respectively. For an azimuthally isotropic air/water interface and assuming the visible frequency (ω_1) and the sum frequency (ω_s) are far removed from electronic resonances, there are only three independent nonvanishing components, $A_{xxz} = A_{yyz}$, $A_{xzx} = A_{yzy} = A_{zxx} = A_{zyy}$, and A_{zzz} [185]. The ω_2 is the infrared input light source, and he L_{ii}'s are defined in terms of the frequency-dependent effective dielectric constant of the interfacial layer, $\epsilon(\omega)$, an air/water interface in our case. For the air/water interface, $\epsilon(\omega_s) = \epsilon(\omega_1) = 1.31$ and $\epsilon(\omega_2) = 1.2$ were estimated [183] from a three-layer model. The numerical values of all these variables can be found in Table 1 of ref. [183]. The A_{ijk}'s are intrinsic (macroscopic) properties of the interface, whereas the experimental observables, A_{eff}'s, are affected by the frequency-dependent dielectric response of the interface medium as described above and by the experimental conditions. Therefore, using Eq 5.2 we obtain A_{eff}'s from the calculated A_{ijk}'s.

The A_{ijk}'s in eq. (5.2) are the resonant components of macroscopic susceptibility tensor, and can be represented at a molecular level as an ensemble average of the molecular hyperpolarizability in the body fixed frame, $\beta_{q,\lambda\mu\nu}$ (corresponding to the hyperpolarizabililty A_q of Du et al. [163]), of the interfacial water molecules in the lab frame (denoted by *ijk*), where q corresponds to the IR resonant mode of the free OH bond. The derivation begins with the Fourier-Laplace transform of the classical SFG response function: related references are [180, 183, 187, 188, 189, 190].

$$\begin{aligned} A_{q,ijk} &\equiv (\omega_2 - \omega_q + i\Gamma_q)\chi^{(2)}_{ijk} \\ &= -(\omega_2 - \omega_q + i\Gamma_q)\frac{i\omega_2}{k_b T}\int_0^\infty e^{i\omega_2 t}\langle \alpha_{ij}(0)\mu_k(t)\rangle \, dt, \end{aligned} \tag{5.3}$$

where α_{ij} is the quantum mechanical instantaneous polarizability tensor of the entire surface, and μ_k is the in instantaneous dipole moment vector of the surface. eq. (5.3) must be converted to be applicable to classical MD simulations. Because we are considering a mode directly on resonance, we introduce the two resonant states of the full basis set, $|0\rangle$ and $|1\rangle$, where, $|1\rangle$ represents the first excited vibrational mode of the free OH-bond at 3700 cm^{-1}. This contributes a factor $\langle 0|\mu(t)\rangle|1\rangle \propto \exp(-i\omega_q t)$. Because the integral in eq. (5.3) will be dominated by the resonance term, we replace

ω_2 with ω_q, the value at the peak. We take the remaining QM expressions to their classical limit [191]. In particular, the orientations of the surface bonds will be given by their classical values, so we may expand eq. (5.3) as

$$\begin{aligned} A_{q,ijk} = &-(\omega_2 - \omega_q + i\Gamma_q)\frac{i\omega_q}{k_b T}\sum_{\lambda\mu\nu}\alpha_{\lambda\mu}\mu_\nu \\ &\times \int_0^\infty e^{i(\omega_2-\omega_q)}\left\langle \sum_n^{N_{OH}(t)}\sum_m^{N_{OH}(t)} D^n_{i\lambda}(0)D^n_{j\mu}(0)D^m_{k\nu}(t)\right\rangle, \end{aligned} \tag{5.4}$$

where the sum of λ, μ, or ν is over $\hat{u}$, $\hat{v}$, or $\hat{w}$, the basis of the body-fixed molecular reference frame. Similarly, $i = \hat{x}, \hat{y}, \hat{z}$, the laboratory frame basis, and the same holds for the j and k. The double sum in eq. (5.4) includes the n^{th} and m^{th} free surface OH bonds at times 0 and t, respectively. At time t there are $N_{OH}(t)$ free OH bonds. $D^n_{i\lambda}$, $D^n_{j\mu}$ and $D^m_{k\nu}$ are the time-dependent direction cosine matrix elements of the n^{th} and m^{th} free surface OH bonds, defined as $D_{xu} = \hat{x}\cdot\hat{u}$. Thus, $\alpha_{\lambda\mu}$ and μ_ν are the mean per-bond body-centered reference frame polarizability and dipole, respectively. eq. (5.4) is a generalization of equations in Wei and Shen [183], and it can be shown to reduce to corresponding approximations of slow and fast orientational dynamics. However, eq. (5.4) also explicity incorporates spatial correlations between water molecules, unlike those in Wei and Shen, who employed a mean-field approximation,[1].

Inspection of eq. (5.3) shows that we may substitute in the bond hyperpolariz-

---

[1] The mean-field approximation is very common in SFG analysis. Most texts, such as Shen's [190] state that the total susceptibility is N times the susceptibility of a single molecule. Although it may make sense to construct an average susceptibility per molecule, it does not necessarily follow that the average susceptibility is the same as the susceptibility of a single, isolated molecule

ability, $\beta_{q,\lambda\mu\nu}$, giving

$$A_{q,ijk} = -(\omega_2 - \omega_q + i\Gamma_q) \sum_{\lambda\mu\nu} i\beta_{q,\lambda\mu\nu} \times \int_0^\infty e^{i(\omega_2-\omega_q)} \left\langle \sum_n^{N_{OH}(t)} \sum_m^{N_{OH}(t)} D^n_{i\lambda}(0) D^n_{j\mu}(0) D^m_{k\nu}(t) \right\rangle . \tag{5.5}$$

We approximate the hyperpolarizability of H_2O at $\omega_2 = \omega_1 = 3698$ cm^{-1} by the "bond hyperpolizability" of the free OH bond with cylindrical symmetry. This assumption accomplishes two things. First, this simplifies eq. (5.5) by converting it to a form that can be evaluated using the experimentally observed bond hyperpolarizability. Second, it allows us to exclusively account for the orientation of the free OH bounds, the quantities that are produced by the simulation. Under this assumption, $\beta_{q,\lambda\mu\nu}$ has only two unique nonvanishing values, $\beta_{\perp,\perp,\|}$ and $\beta_{\|,\|,\|}$, where $\perp$ and $\|$ denote the body-fixed axes along and perpendicular to the free OH bond direction. To explain this restriction, we consider how the incoming lasers interact with the underlying symmetry of the cylindrical bond. The bond has broken symmetry along its axis, from the O to the H, but it is symmetric under rotation around the OH axis. When the third component of the hyperpolarizability tensor, which represents the IR beam, is perpendicular to the axis, $\perp$, the IR laser interacts with the part of the bond that is symmetric under rotation and centrosymmetric, so the intrinsic susceptibility from the IR is 0. When the IR beam is parallel, $\|$, it is interacting with the noncentrosymmetric part of the cylindrical bond, so it has nonzero value. The visible beam is far off resonance, so the bond has nearly zero coupling, hence the bond looks symmetric from all directions. This means the visible laser cannot drive the SFG on its own, so the IR beam must be $\|$, giving $\beta_{,,\perp} = 0$. Because the frequency of the visible laser is chosen to be far from any electronic resonances, the susceptibility at ω_1, the incoming visible laser frequency, and $\omega_s = \omega_1 + \omega_q$, the outgoing SFG frequency, are nearly identical, because the susceptibility has small variance far away from resonance. Hence, we have $\chi_{ijk}(\omega_s, \omega_1, \omega_w) = \chi_{jik}(\omega_1, \omega_s, \omega_2) \approx \chi_{jik}(\omega_s, \omega_1, \omega_2)$. This is called Kleinman's symmetry [113], and it means that first and second components of the hyperpolizability must be identical. Thus, the only nonzero components correspond to $\beta_{\perp,\perp,\|}$ and $\beta_{\|,\|,\|}$. Using Raman and IR measurements, these values have been measured [163, 183]:

$$\beta_{\|} \equiv \beta_{\|,\|,\|} = \beta_{www} = 2.88 \times 10^{-27} \, \frac{\mathrm{m}^5}{\mathrm{Vs}}, \text{ and}$$
$$\beta_{\perp} \equiv \beta_{\perp,\perp,\|} = \beta_{uuw} = \beta_{vvw} = 0.32\beta_{\|}.$$

Therefore, the sum over (λ, μ, ν) only has three nonvanishing combinations: $(\hat{u}, \hat{u}, \hat{w})$, $(\hat{v}, \hat{v}, \hat{w})$, and $(\hat{w}, \hat{w}, \hat{w})$.

The time-dependent direction cosine matrix is $D_{\ell\zeta} = \hat{\ell} \cdot \hat{\zeta}$, with $\hat{\ell} = (\hat{x}, \hat{y}, \hat{z})$ the fixed lab coordinates and $\hat{\zeta}(t) = (\hat{u}, \hat{v}.\hat{w})$ are the time-dependent molecular coordinates of the free OH bond. The water surface normal is along the z-axis of the laboratory coordinates, and a free OH bond forms an angle $\theta(t)$ with the surface normal at time t. The angle $\theta(t)$ lies in the interval $[0, \pi]$, and the angle with respect to $\hat{x}$ in the $\hat{x}.\hat{y}$ plane, $\phi(t)$ is in the interval $[0, 2\pi]$. The the full expression of the molecular coordinates in terms of laboratory coordinates is

$$\hat{u} = \cos\phi\cos\theta\,\hat{x} + \sin\phi\cos\theta\,\hat{y} - \sin\theta\,\hat{z} \tag{5.6a}$$

$$\hat{v} = -\sin\phi\cos\theta\,\hat{x} + \cos\phi\cos\theta\,\hat{y} - \sin\theta\,\hat{z} \tag{5.6b}$$

$$\hat{w} = \cos\phi\sin\theta\,\hat{x} + \cos\phi\cos\theta\,\hat{y} + \cos\theta\,\hat{z}. \tag{5.6c}$$

$$\tag{5.6d}$$

To evaluate the error introduced by finite simulation snapshot time interval, three MD simulations with different snapshot time intervals were used for the calculations, as described below.

In the MD simulations, 1264 water molecules were placed in a rectangular box of dimension $30 \times 30 \times 70$ Å^3 where the water section is sandwiched between two sections of vapor along the z-axis. Periodic boundary conditions were used in all directions, but, along the z-axis, we sandwiched the water slab with two slabs of vacuum. Water molecules were modeled by the DL_POLY 2 program [192] as rigid and nonpolarizable, using the TIP3P potential commonly used for molecular mechanics [193]. The Nosé-Hoover thermostat [194, 195] was used to perform the constant NVT MD simulations at T = 298 K, and the SHAKE algorithm [196] was used to constrain the degrees of freedom of rigid water molecules. The time step for integrating Newtons equations is always 1 fs, but it is unnecessary to record the results of each step. Instead, we recorded the instantaneous orientation of all free OH bonds in discrete snapshots, evolving the simulation between snapshots without recording the individual steps. In this work, we saved all of the configurations for the snapshot time interval of 1 fs, and every 10 configurations for a time interval of 10 fs, and every 100 configurations for 100 fs. After adequate equilibration of a random initial configuration, simulated with a time step of 1 fs, three individual simulations each with a different snapshot time interval of either 1 fs, 10 fs, or 100 fs were performed. In the three cases, to generate a total of 40,000 configurations, the total simulation time was 40 ps, 400 ps, and 4 ns, respectively. The correlation functions were calculated using a time average,

$$C(t) = \langle \alpha(0)\mu(t) \rangle = \frac{1}{N+1} \sum_{n=0}^{N} \alpha(n\delta t)\mu(t + n\delta t),$$

where $N = (T - t)/\delta t$. T is the total length of the simulation, and δt is the time step of the simulation results.[2] The results are shown in figure 5.3.

For sampled configurations of the water/vacuum interface, it is essential to select only the free OH bonds on the water surface that respond to the laser beams in real SFG experiments. Only the free OH bonds at the surface will break the inversion symmetry necessary for an SFG signal. Previous simulation studies [157, 169, 159, 171, 172] identified surface free OH bonds as those positioned above a certain cutoff in the z-direction. However, as can be seen in figure 1, the water surface in the model fluctuates appreciably, and an arbitrary cutoff unavoidably includes the OH bonds in the bulk. Although isotropy due to random orientation of the free OH bond in the bulk will provide a natural surface selection effect, the local field corrections relevant

---

[2] This time average is equivalent to the ensemble average on the limit $T \to \infty$. If the simulation were to not fully explore the phase space, the correlation function can develop artifacts due to over representation of some simulation behavior. If an ensemble average is used, the solution is to add more simulations.

to calculating A_{eff}'s only apply to the free OH bonds directly on the surface [197]. The correct selection procedure would be to select only those free OH bonds that are both on the surface and those that do not contribute to bulk inversion symmetry. This aspect led us to exclude surface free OH bonds oriented toward the bulk and keep those oriented toward the vapor. Two experimental quantities, the surface density of free OH bonds [198], $N_s = 2.8 \times 10^{18}$ m^2, and their average tilt angle [163, 168, 183] of about 35°, guided us in determining free surface OH bonds that affect the SFG results. In this study, the following three criteria were combined to select the free surface OH bonds which lead to agreement with the above two experimental quantities. First, an OH bond is considered on the surface if no oxygen atoms are inside the open cylindrical space above the hydrogen atom with a radius of 1.5 Å(roughly the length of an OH bond). Second, the OH bond is not H-bonded with any oxygen atoms. An OH bond is considered H-bonded with another oxygen atom if the interoxygen distance is less than 3.5 Å(first coordination shell) and simultaneously the $\mathrm{O - H \cdots O}$ angle is less than 30° (approximate librational wagging amplitude of the H-bonds) [199]. Because of approximations in the dielectric model, some free OH bonds may be inappropriately included. If the bond is oriented with a large angle to the surface normal, in reality it would have a high probability to be effectively canceled out by another OH bond pointing in the opposite direction. Our selection method must produce an orientation ensemble that reflects this potential inversion symmetry. To address this feature, we used a single free parameter in the calculations, a free OH cutoff angle. Bonds with θ_{OH} greater than the cutoff angle were not included in the calculations.

A snapshot of the free surface OH bonds is shown in figure 5.1(b). Clearly, the free surface OH bonds in the model are sparse and their oxygen atoms do not form a uniform monolayer. The distribution of the cosine function of the tilt angle θ with respect to the surface normal is plotted in figure 5.2. As expected, the three snapshot intervals do not yield a large difference in the cosine distribution, because of the equilibrating prior to the simulation. Because a cutoff of 60° was applied to the tilt angle, $\cos\theta_{OH}$ cannot be smaller than 0.5, as observed in figure 5.2. The plurality of free OH bonds is oriented along the surface normal.

With the surface free OH bonds determined, the A_{eff}'s were calculated using Eqs. (5.3) – (5.4). Because the experimentally determined values of the A_{eff}'s were determined by fitting the observed spectra to Lorentzians [183], the spectra calculated with the simulation results were also fit to Lorentzians. That is, after calculating the correlation functions, by using eq. (5.4), we calculate the Fourier-Laplace transforms at all ω_2 to obtain a spectral response. These Fourier-Laplace transforms are then corrected to account for local field corrections, as in eq. (5.2), leading to the frequency-dependent susceptibilities $\chi_{ssp}(\omega)$, $\chi_{ppp}(\omega)$, and $\chi_{sps}(\omega)$. To arrive at the A_{eff}'s, we take the absolute value of the susceptibilities, as these are the quantities measured in the experiments. The spectra are fit to Lorentzians, $a^2/((\omega-\omega_q)^2+\gamma^2)$, thereby extracted a and γ. The constant a is the correlation function $\langle\alpha(0)\mu(t)\rangle - \langle\alpha\mu\rangle_{\text{final}}$ evaluated at $t=0$, where $\langle\alpha\mu\rangle_{\text{final}}$ is the baseline of the plot. The value of a is determined only by the equilibrium properties and is insensitive to the detailed dynamics, while the dynamics lie in Γ_q (and γ).

The γ which is extracted from our simulation cannot be the same as Γ_q. First, a brief consideration of the correlation functions in figure 5.3 shows the decay times are on order 0.1 picoseconds, while experimentally observed decay times are closer to 1 picosecond, differing by two orders of magnitude. This discrepancy is due to the binary classification of free surface OH bonds. Bonds may appear and disappear extremely rapidly. In reality, the bond's ω_q would drift in concert with its exposure, equaling 3698 cm^{-1} when free and moving smoothly and continuously to other frequencies as it form bonds with its neighbors. Thus, the experimentally observed bonds will have a much longer correlation time. Even so, we expect the amplitude, a, to be unaffected by the this binary selection procedure, as we successful capture the equilibrium properties. Hence, as expected, a correlation time that is too small corresponds to a spectral width that is far too wide.

Therefore, what we are calculating is not A_{ijk} but a quantity better labeled as A_{MD}, originating from $\chi^{(2)}_{MD}$. We define $\alpha = A_{ijk}/A_{MD}$. Because we have defined the spectrum of $\chi^{(2)}_{MD}$ to have a peak at ω_q, and because we observe it to be largely Lorentzian in nature, we know

$$\begin{aligned}\alpha^2 &= \frac{A^2_{ijk}}{A^2_{MD}} \\ &= \frac{\Gamma_q \int |\chi^{(2)}_{ijk}(\omega)|^2}{\gamma \int |\chi^{(2)}_{MD}(\omega)|^2}.\end{aligned} \tag{5.7}$$

We can see in eq. (5.7) that the relative areas under the curve in the spectra determine the final value of α. By Parseval's Theorem, $\int_{-\infty}^{\infty} |\chi^{(2)}_{ijk}(\omega)|^2 d\omega = \int_{-\infty}^{\infty} \delta C^2_{ijk}(t) dt$, where

$\delta C(t)$ is the mean-subtracted correlation function. Because the mean-subtracted correlation function is also the impulse response function, the integrals are the total power produced following a delta-function input pulse. We assume that the two powers produced are identical.[3] Therefore, $\alpha = \sqrt{\Gamma_q/\gamma}$, which we will use as a correction factor. We then have

$$A_{\text{eff}} = \sqrt{\frac{a}{\Gamma_q \gamma}}.$$

We divided by Γ_q to account for the fact that its built into the β_{ijk}, which comes from an experimental measurement. The resulting corrected amplitudes are shown in Table 5.2. All ratios of the calculated mode amplitudes are nearly within the measured error of the experimental ratios $A_{\text{eff}}(ssp)\colon A_{\text{eff}}(ppp)\colon A_{\text{eff}}(sps) = 1\colon 0.28 \pm 0.04\colon 0.05 \pm 0.02$.

The largest amplitudes in Table 5.2, the $A_{\text{eff}}(ssp)$ and $A_{\text{eff}}(ppp)$, correspond to the incident IR laser being p-polarized. In p-polarization, the electric field vector is parallel to the plane of incidence and therefore probes free OHs that are nearer to the surface normal, and these free OHs are those with the most orientational anisotropy. The $A_{\text{eff}}(ssp)$ is about three times larger than the $A_{\text{eff}}(ppp)$, perhaps reflecting the factor of three difference between $\beta_{\perp}$ and $\beta_{\parallel}$. The $A_{\text{eff}}(sps)$ is smaller than the other two, presumably because with the incident s-polarization, the IR tends to probe free OHs that are closer to being flat on the surface.

---

[3] This is a major assumption. One way to justify it may be as follows: Let's assume the simulation fully captures the rotational dynamics and the symmetry breaking at the surface. Because this is the symmetry breaking responsible for the SFG, we can assume it to be independent of the other modes we have neglected. Effects such as motional narrowing, which may be particularly strong at the surface due to rapid change in electric field, may have the effect of slowing down surface dynamics without altering the total time-averaged asymmetry.

5.2 Results and Discussion

The detailed information of the microscopic structure and dynamics of water/vacuum interface provided by the computer simulations provide some insight into the physical meaning of the three experimental observable mode amplitudes, the average orientation, and free OH bond surface density. Our results, shown in Table 5.2 achieve good agreement with observed ratios, and they are also within an order of magnitude of experimentally measured results. Because the 1 fs snapshot interval led to a total integration time of 40 ps, which may be too short to adequately generate statistics (others have used multiple nanoseconds [187]), those results would expectedly differ from the longer simulation times. Although Wei and Shen obtained agreement in the calculated ratios of $A_{\text{eff}}(ssp) : A_{\text{eff}}(ppp)$ by assuming the rotational dynamics of θ_{OH} are very fast compared to the vibrational lifetime, they arrived at precisely $A_{\text{eff}}(sps) = 0$ [183]. Our calculations produce a small but nonzero $A_{\text{eff}}(sps)$, which we plan to investigate more fully comparing the slow approximation limit of the present equations. We will determine this further in future calculations. Although Gan et al. [168] suggest the free OH bonds rarely orient perpendicularly to the surface, their results assumed the distribution of angles to be Gaussian, with a width of about 15 degrees, instead of using a distribution similar to the one calculated in figure 5.2. By calculating the distribution of the bonds and employing a cutoff, we obtain good agreement in the ratio of effective susceptibilities. We also show that not all free OH bonds are necessarily SFG active, and this may be a source of discrepancy between theoretical measurements of bond orientations and the narrower results from experiments [168]. As expected, $A_{\text{eff}}(ssp)$ is the largest component because it represents the IR laser coupling directly to the component of the free OH bond oriented perpendicularly to the surface, the orientation with the largest anisotropy. Future work will reveal more information when we extend the overall results and compare them with the slow and fast approximations of the present equations. Based on the present MD simulations of the air/water interface with the TIP3P empirical water model, the amplitudes and their ratios of the effective nonlinear susceptibilities (A_{eff}s) were calculated for different polarization combinations and compared with sum-frequency generation (SFG) experiments. Free surface OH bonds are selected as the OH bonds (1) which are not hydrogen-bonded to other oxygen atoms; (2) whose title angles with respect to the surface normal are smaller than 60°; and (3) no oxygen atoms are above the hydrogen atom. With this definition of free surface OH bonds, the calculated average surface density and average tilt angle closely match the experimental values. The calculated absolute values of the experimental observable mode amplitudes differ, while the ratios are relatively similar. The water model presented here was utilized to capture the dynamic orientational distribution of surface free OH bonds. Although the present water model, TIP3P, may be satisfactory for predicting dangling surface OH bonds, there are indications from unpublished work that it predicts too many dangling OHs in bulk water, compared with experiments for nonbonded OH bonds. Measurements of nonbonded OHs in bulk water have been reported by Eaves et al. [200]. For studies of bulk reaction dynamics, an alternative to the TIP3P model should be explored. We are investigating how the SPC/E model [201], which has been used for bulk water structure, will alter the calculated susceptibilities. Due to the SPC/E model being better at predicting bulk water properties, we expect the enhanced correlation to bring the susceptibilities even closer to experimental results. We have not considered the effects of capillary fluctuations on the calculated effective susceptibilities, and this will be investigated in a future publication on SFG. In addition, future simulations calculating ensemble averages of correlation functions, instead of effective time averages, may reduce artifacts leading to variations in the calculated susceptibilities between snapshot lengths. This simulation study adds to the theoretical insight into the microscopic structure of the vacuum/water interface, and the present results provide useful information in supporting the recent theory of on-water heterogeneous catalysis [182].

5.3 Conclusion

In summary, we have formulated the SFG equations in a form where molecular dynamics (MD) calculated quantities can be directly compared with hyperpolarizability (polarizability-dipole) coefficients, A_{eff}, extracted from the experimental data for different types of polarization combinations of the infrared, visible, and reflected light. Preliminary MD results were obtained and the extracted information compared with the experimental data, both in the comparison of ratios of A_{eff}s and also for comparison with their absolute values. The SFG results were interpreted in terms of physical concepts, for use in exploring other issues and with additional water models. Data from independent sources, infrared and Raman experiments, has been used, in

Table 5.1: Average number of free surface OH bonds, $\langle N_{OH} \rangle$, and average orientation angle, $\langle \theta_{OH} \rangle$, of free surface OH bonds calculated from three MD simulations with different snapshot time intervals

Snapshot interval	$\langle N_{OH} \rangle$	$\langle \theta_{OH} \rangle$
1 fs	26	38°
10 fs	26	38°
100 fs	26	38°

conjunction with SFG theory, to calculate the SFG susceptibility coefficients. In this way, the overall SFG problem was divided into two parts, rather than calculating *ab initio* the quantum mechanical values of the dipole moment and polarizability derivative. They, in practice, can be computed separately or, as above, evaluated from independent experimental data.

Table 5.2: Results of fitting the calculated spectrum to a Lorentzian and correcting for experimental width.

Mode Amplitudes (10^{-9} $\mathrm{m^2\,V^{-1}s^{-1}}$)	1 fs	10 fs	100 fs	Experiment
$A_{\text{eff}}(ssp)$	3.19	1.23	2.95	1.7
$A_{\text{eff}}(ppp)$	0.96	0.38	0.9	0.48
$A_{\text{eff}}(sps)$	0.05	0.02	0.026	0.09
$ssp : ppp : sps$	1:0.30:0.02	1:0.31:0.02	1:0.30:0.01	1:0.28±0.04:0.05±0.02

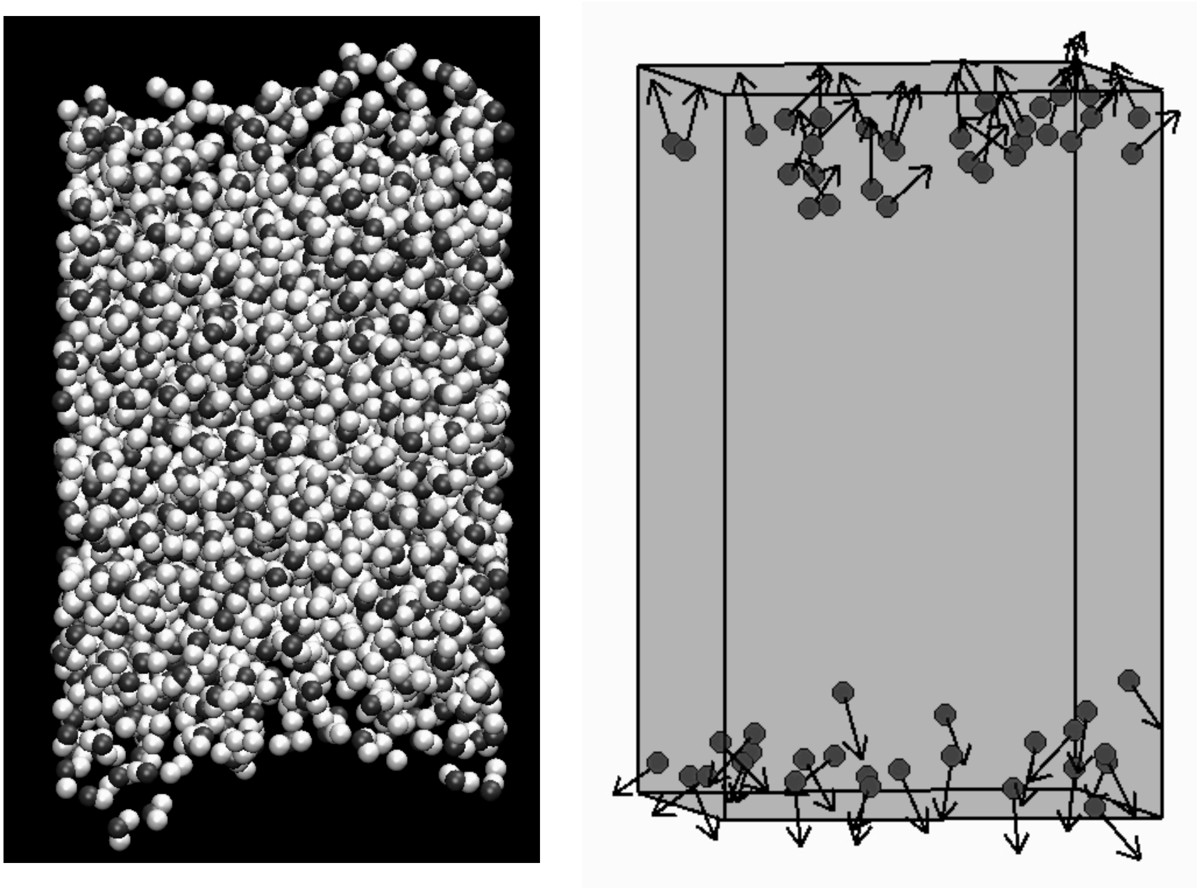

(a)

(b)

Figure 5.1: (a) Snapshot of the simulated water/vacuum interfaces. Black spheres represent oxygen atoms, and white ones represent hydrogen atoms. (b) Snapshot of the chosen free surface OH bonds. Black spheres represent oxygen atoms and the vectors point from oxygen atoms to the bound hydrogen atoms. The vectors are elongated for clearer illustration.

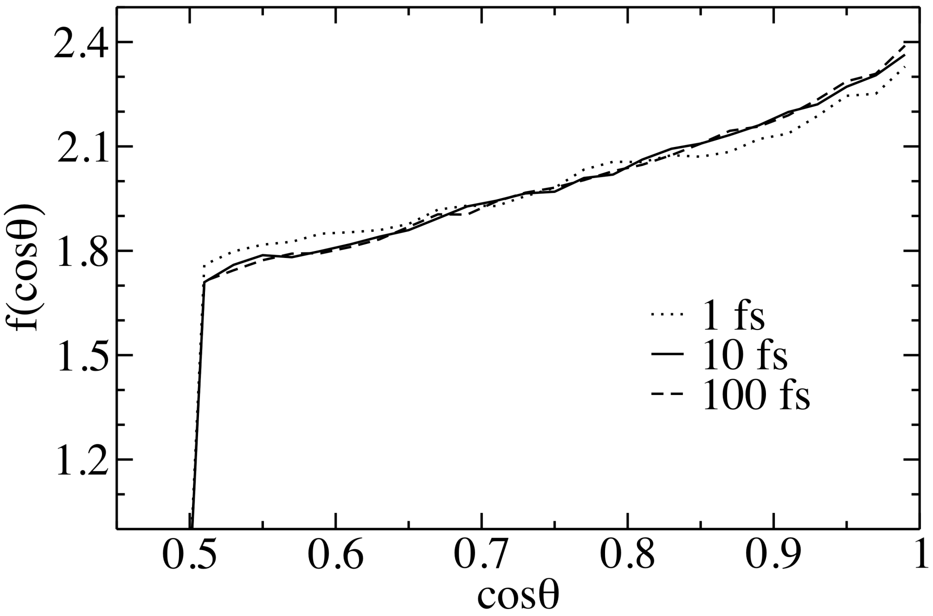

Figure 5.2: Probability density of the cosine of the tilt angle with respect to the surface normal, using a cutoff angle of 60°. The three MD simulations with different snapshot intervals of 1, 10, and 100 fs, respectively, result in very similar cosine angle distributions.

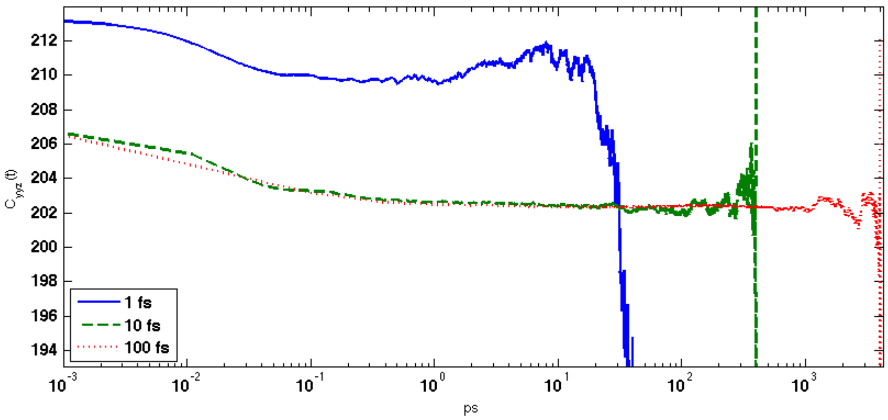

(a) $C_{yyz}(t)$

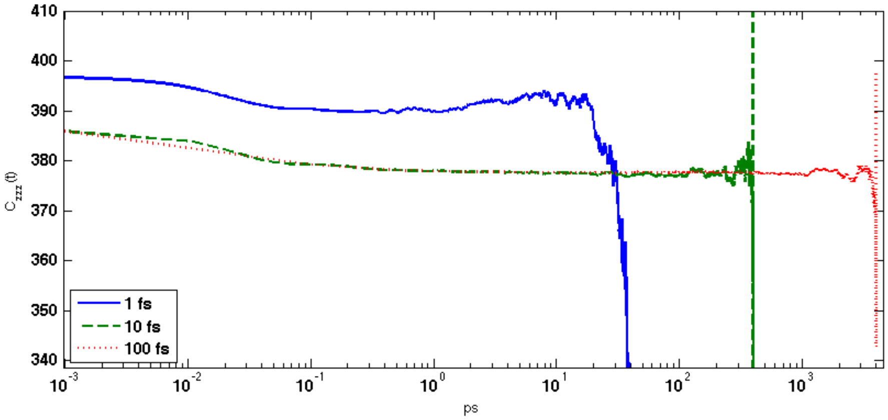

(b) $C_{zzz}(t)$

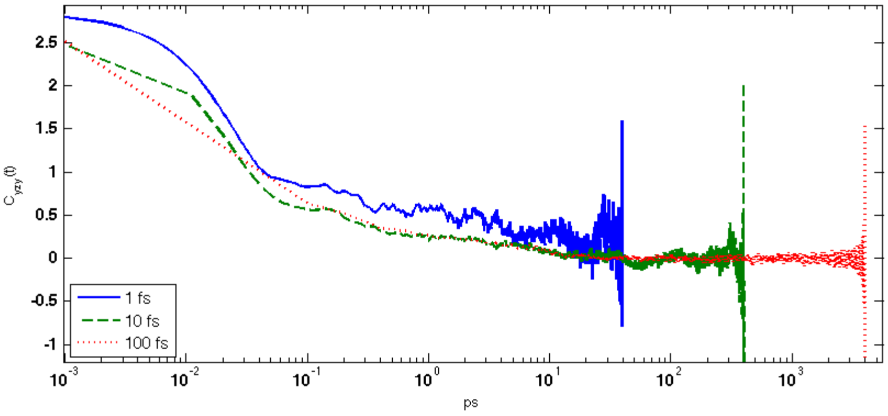

(c) $C_{yzy}(t)$

Figure 5.3: Correlation functions of free OH bonds produced by simulation, using three different snapshot times, 1 , 10 , and 100 fs. Note the semi-log x-axis, which is in picoseconds.